Rare Metal Materials and Engineering
Volume 49, Issue 12, December 2020
Available online at www.rmme.ac.cn

Science Press

Cite this article as: Rare Metal Materials and Engineering, 2020, 49(12): 4041-4049.

ARTICLE

Influence of Rotation Angle on Cold Rolling Forming Process of AZ31 Magnesium Alloy Tubes

Xue Chun[1], Chu Zhibing[1,2], Su Hui[1], Li Wei[1], Li Yugui[1], Ma Lifeng[1]

[1] Engineering Research Center Heavy Machinery Ministry of Education, Taiyuan University of Science and Technology, Taiyuan 030024, China; [2] School of Mechanics and Civil Engineering, Jinan University, Guangzhou 510632, China

Abstract: Cold-rolled AZ31 magnesium alloy tube was used as the research object. Based on the cold-rolling process under different rotation angles, the effects of different rotation angles on the characteristics of equivalent stress, equivalent plastic strain and node temperature during deformation were investigated. Results shows that increasing the rotation angles can increase the equivalent stress, equivalent plastic strain and node temperature. With the aid of the automaton model and experimental means, through the contrast analysis of experiment and numerical simulation results, the preliminary structure evolution law of continuous recrystallization and refinement in the rolling process was analyzed. The results reveal that a 50° rotation angle can meet the technical requirements and provide evidence for the appropriate selection of rotation angles for cold-rolled magnesium alloy tubes.

Key words: three-roll cold rolling; rotation angle; numerical simulation; cellular automaton

The three-roll cold-rolling seamless pipe processing method, as a typical reciprocating multichannel rolling procedure, simultaneously achieves multi-pass rolling and small single-pass deformation; moreover, this method can extensively refine grains and improve the grain orientations to eliminate microstructural defects and improve mechanical properties[1]. Superior-performance seamless metal steel tubes can be obtained with high dimensional accuracy in the production of high strength and low plasticity of seamless steel tubes, and they occupy an irreplaceable position[2,3]. Domestic and foreign scholars have prepared refractory metals using three-roller cold-rolling[4-7].

Danchenko et al[8] studied metal flow in the Pilger rolling process under different process parameters, and proposed a new calculation method for the cold Pilger rolling model. Montmitonnet[9] simulated the forming process of Pilger rolling and studied the influence of process parameters on the size of the resulting tube. Abe et al[10] conducted an analytical study of rolling conditions, which affects the size accuracy and ovality of pipes obtained via the cold Pilger rolling process. Huang et al[11,12] studied theoretical and plastic deformation behavior, and conducted modeling and validation for three-dimensional multi-strokes cold pilgering of TA18 titanium alloy tube. However, these studies only reveal the characteristics and rules of tube formation in two-roll cold-rolling and rarely involve the effects of process parameters on the forming characteristics of three roll cold-rolling tubes.

In the actual production, rotation angle selection is based on the rolling materials and production experience. If the selected rotation angle is inappropriate, the resulting pipe will have uneven wall thickness and ovality of its outer diameter. Flash and rolling cracks may also be generated. Therefore, selection of the rotation angle has an important impact on size accuracy and product performance of the finished tube. Based on this condition, cold-rolled AZ31 magnesium alloy tube was us as the research object. Numerical simulation, cellular automaton modeling and experimental studies were conducted to determine the effect of different rotation angles on the forming regularity and microstructural evolution of cold-rolled tubes.

Received date: December 17, 2019
Foundation item: National Natural Science Foundation of China (U1710113); National Key R&D Program of China (2018YFB1307902); China Postdoctoral Science Foundation (2017M622903); Key Research and Development Program of Shanxi Province (201703D111003, 201703D111002, 201703D121008); Joint Postgraduate Training Base of Shanxi Province (2018JD33); Postgraduate Education Innovation Program of Shanxi Province (2019SY482)
Corresponding author: Chu Zhibing, Ph. D., Professor, Engineering Research Centre Heavy Machinery Ministry of Education, Taiyuan University of Science and Technology, Taiyuan 030024, P. R. China, E-mail: 16337296@qq.com

The aim of this study is to recommend a reasonable rotation angle that meets technical requirements and supports the development of cold-rolled AZ31 magnesium alloy pipes.

1 Three-Roll Cold-Rolling Characteristics

1.1 Working principle

Fig.1 shows the three-roll cold-rolling working principle[13]. The roller performs periodic rotation on a fixed track on the roller table. As the roller moves to the end of the track (that is, the final position), the pipe is pushed forward for a certain distance along the rolling direction and rotated at a certain angle (that is, the rotation angle). As the roller moves to the front end of the track (that is, the initial position), the tube billet moves forward a certain distance and turns at an angle until the roller returns to the final position. The process is repeated to realize the cycle rolling process of the tube.

1.2 Metal flow rule in the forming process

Fig.2 shows the schematic of the simulated periodic rolling tube forming movement. The displacement of the tube increases gradually along the rolling direction. The pipe rolling along the direction of displacement increases gradually, the node (target point) on the pipe moves in a spiral motion under the action of the roller, and the spiral radius decreases gradually because the friction among the tube, the roller and the mandrel cause the metal to flow in the rolling direction, circumferential force causes the metal to flow in the circumferential direction, and radial pressure causes the metal to flow in the center of the pipe. These all illustrate the evenness of multi-pass cycle cold rolling deformation[14].

1.3 Cellular automaton model

Cellular automata discretize the complex process of grain change in continuous time and space. Specifically, cell was used to realize the discretization of space, and time step was used to realize the discretization of time by adopting deterministic or probabilistic transition rules between time steps and cells, and the complex grain change process was simulated[15].

The cellular automata consist of five main parts, namely, cell, cell space, cell state, cell neighbor type and transition rules. The relationship between these five parts is shown in Fig.3[16].

1.4 Dynamic recrystallization model based on cellular automata

Based on dynamic recrystallization theory[17], a cellular model was established to simulate the dynamic recrystallization of magnesium alloys. This model combines the dislocation density model, critical dislocation density model, nucleation rate model and grain growth model.

The dislocation density model is a function used to calculate the internal dislocation and strain of grains and introduce the Kocks and Mecking models[18], as shown in Eq.(1) and Eq.(2).

$$\sigma=\alpha\mu b\sqrt{\bar{\rho}} \quad (1)$$

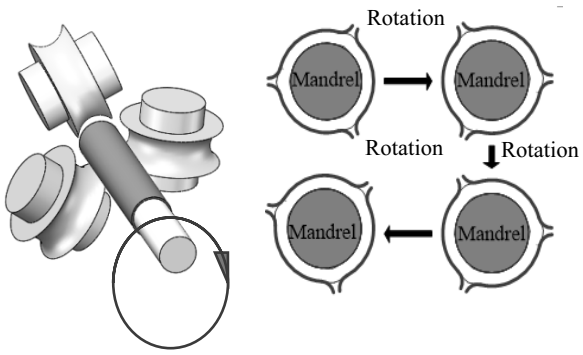

Fig.1 Working principle diagram of three-roll cold-rolling

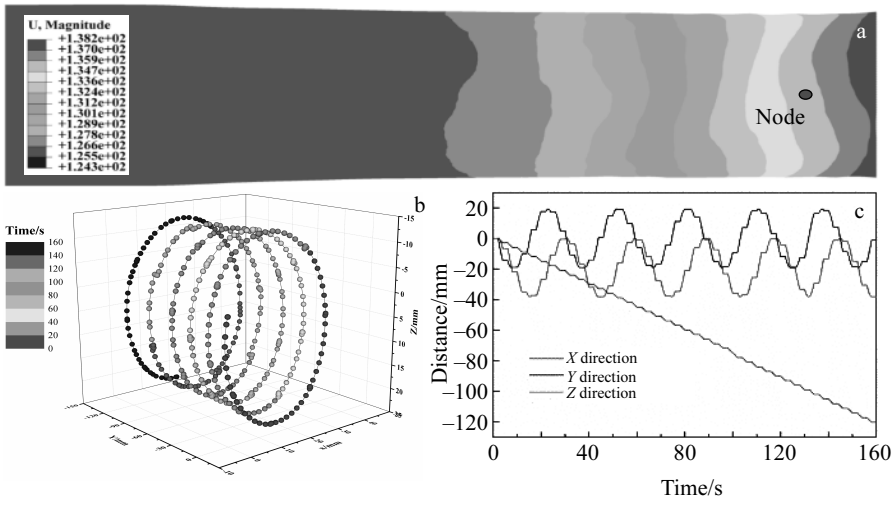

Fig.2 Schematic of the simulated periodic rolling tube forming movement: (a) node displacement cloud map of the deformation zone, (b) node movement in the forming process, and (c) the pipe movement amplitude

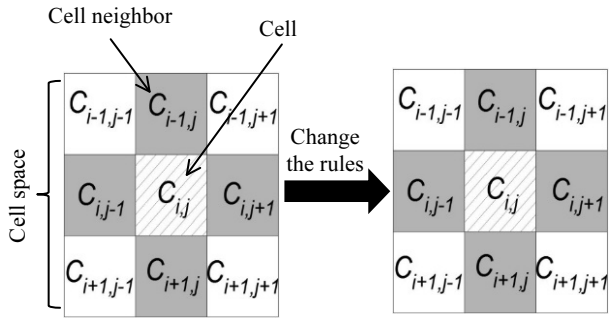

Fig.3 Main components of cellular automata

$$\frac{\mathrm{d}\rho_{ij}}{\mathrm{d}\varepsilon}=k_1\sqrt{\rho_{ij}}-k_2\rho_{ij} \quad (2)$$

where σ is the rheological stress, α is the material constant, $\overline{\rho}$ is the average dislocation density function, μ is the shear modulus, b is the Burgers vector, ε is the strain, k_1 is the dislocation augmentation factor, k_2 is the dislocation extinction coefficient and ρ_{ij} is the cell mean dislocation density

$$\rho_{\mathrm{c}}=\left(\frac{20\gamma_i\varepsilon}{3blM\tau^2}\right)^{1/3} \quad (3)$$

where ρ_{c} is the critical dislocation density, γ_i is the grain boundary energy, l is the mean free length of dislocation, τ is unit dislocation energy and M is the grain boundary mobility.

The number of new nuclei created is calculated according to the nucleation rate model, expressed by Eq.(4):

$$n(\varepsilon,T)=C\varepsilon^m\exp\left(-\frac{Q_{\mathrm{act}}}{RT}\right) \quad (4)$$

where $n(\varepsilon,T)$ is the nucleation rate and C and m are material parameters. Methods to determine C include the experimental method[19] and the inverse analysis method[20]. The present research used the inverse analysis method to determine C.

New nuclei continue to grow under the influence of heat and strain deformation, and the migration speed can be calculated according to Eq.(5):

$$V=MP \quad (5)$$

where V is the grain growth rate and P is the driving force of grain growth per unit area.

2 Numerical Simulation Results

Fig.4 shows a schematic of selected measurement point for different deformation sections. The three sections of the rolling process are symmetrical to the centre of the tube, and each part is 120°. Therefore, based on the circumferential direction of the pipe and contact position of the roller, the data of seven points are intercepted and then analyzed corresponding to other two parts. The rolling direction is taken according to the position of the analysis step corresponding to the characteristic section. In the present research, three sets of numerical models under different rotation angles are simulated;

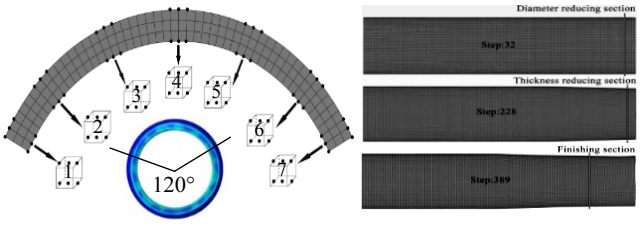

Fig.4 Location of the numerical simulation model

rolling process parameters obtained from the actual production of an enterprise in Jiangsu province are shown in Table 1.

2.1 Effect of equal force distribution under different rotation angles

Fig.5 shows the equivalent stress distribution curves of each characteristic deformation section at different rotation angles, revealing the equivalent stress distribution curves of the reducing, wall thickness reducing and finishing sections. Comparison of the equivalent stress distribution curves of different positions demonstrates that the maximum equivalent stress inside and outside the reducing section and wall thickness reducing section appears at the ridge of the pass, whereas the maximum equivalent stress of the finishing section occurs at the opening of the pass during rolling. According to the equivalent stress distribution curves of different deformation stages, under changes in rotation angle, the change trend of the equivalent stress at the ridge of the pass is larger than that of the opening area of the pass when the pipe and roll are not in contact. According to the equivalent stress distribution curves of different deformation stages, it can be concluded that under the same turning angle, the overall equivalent stress of the outer wall is larger than that of the inner wall, and the overall equivalent stress of the wall thickness reducing section is larger than that of the reducing and finishing sections, regardless of the pass type. The equivalent stress increases with increasing the rotation angle. Therefore, choosing an appropriate rotation angle is vital in ensuring production efficiency and saving cost and energy.

Fig.6 shows the cross-sectional stress nephograms and distribution diagrams of the reducing (Fig.6a), wall reducing (Fig.6b) and finishing sections (Fig.6c). During cold rolling deformation, the stress state at the ridge of the pass is composed of axial tensile stress σ_{l}, circumferential compressive stress σ_θ, and free radial stress σ_{r} into axial compressive stress σ_{l}, circumferential compressive stress σ_θ and radial compressive

Table 1 Rolling process parameters

Number of rack travel/time·min^{-1}	Rolling speed/ mm·s^{-1}	Roll diameter/ mm	Rotation angle/(°)
60	800	55.94	39/50/59

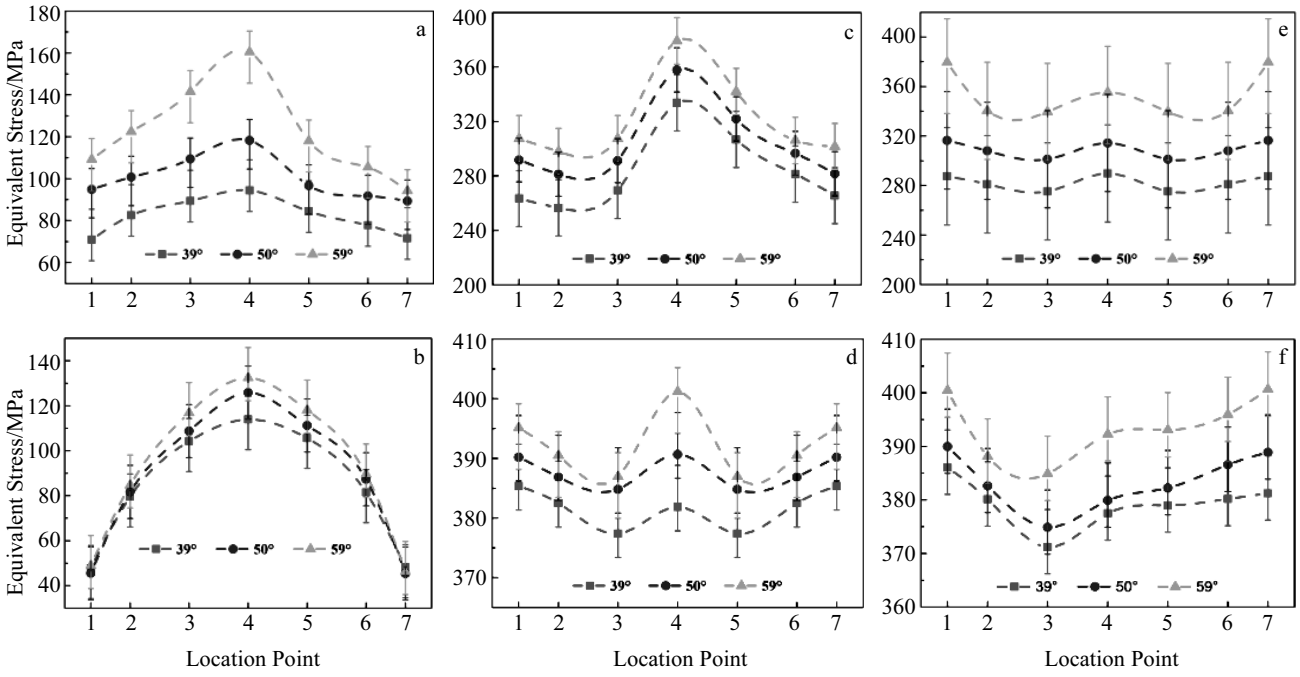

Fig.5 Equivalent stress distribution curves of the outer wall (a, c, e) and inner wall (b, d, f) of different sections at different rotation angles: (a, b) diameter reducing section, (c, d) wall thickness reducing section, and (e, f) finishing section

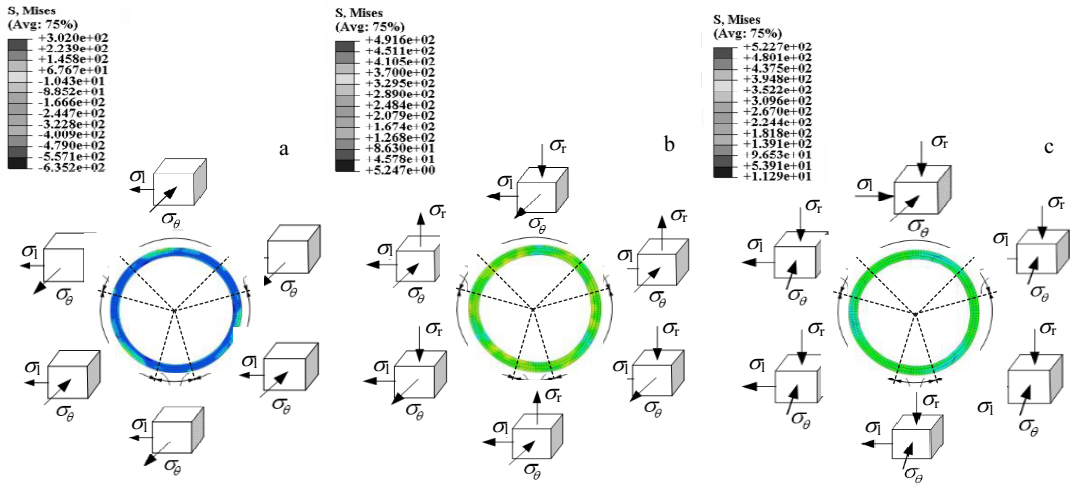

Fig.6 Stress nephograms and distribution diagrams of different deformation sections: (a) reducing section, (b) wall thickness reducing section, and (c) finishing section

stress σ_r. At the opening of the pass, the stress state is composed of axial tensile stress σ_l, circumferential tensile stress σ_θ, and free radial stress σ_r into axial tensile stress σ_l, circumferential compressive stress σ_θ and radial compressive stress σ_r. The stress nephogram distribution can be characterized by the following comprehensive analysis. The reducing section has the least stress, and its maximum stress is distributed at the ridge of the groove. The maximum stress is observed in the wall thickness reducing section and mainly distributed evenly around the ridge of the pass. The stress distribution in the finishing section is uneven, and the maximum stress is distributed at the opening of the pass. The overall stress variation law is in accordance with the distribution curve of the equivalent stress during cold rolling forming.

2.2 Strain distribution under different rotation angles

Fig.7 reveals the equivalent plastic strain distribution curves of the reducing section, wall thickness reducing section and

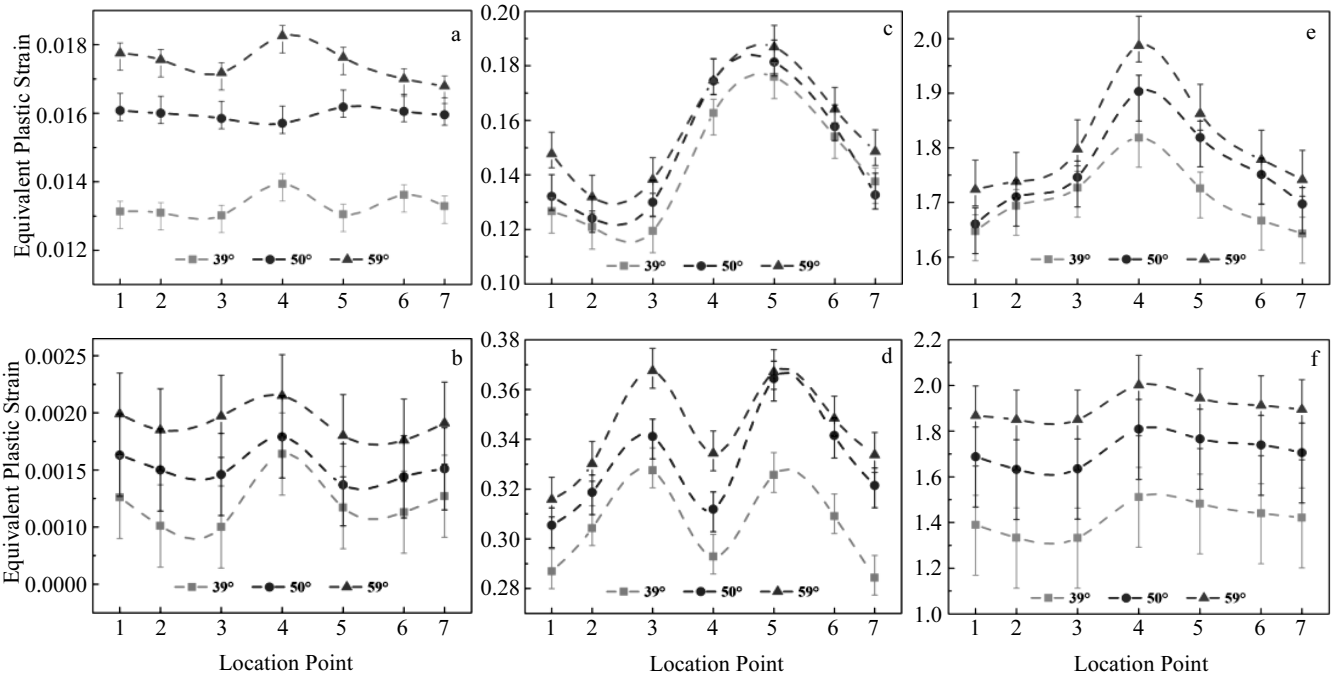

Fig.7 Equivalent plastic strain distribution curves of the outer wall (a, c, e) and inner wall (b, d, f) of different sections at different rotation angles: (a, b) diameter reducing section, (c, d) wall thickness reducing section, and (e, f) finishing section

finishing sections at different rotation angles. The equivalent plastic strain of the reducing section is small, and extensive plastic deformation does not occur. In addition, the distribution is relatively uniform. During rolling, the equivalent plastic strain of the wall thickness reducing section increases, but the strain distribution is not uniform in each area of the pass. After entering the finishing section, the strain reaches the maximum value and becomes more uniform. Comparison of the equivalent plastic strain distribution curves in different deformation stages demonstrates that the equivalent plastic strain increases as rotation angle is increased in any area of the pass, and the increasing trend of reducing and finishing section is relatively uniform as a whole compared to the wall thickness reducing section. Due to the accumulation of equivalent plastic strain, the equivalent plastic strain of the finishing section is larger than that of the wall thickness reducing section and reducing section. Furthermore, the equivalent plastic strain of the finishing section is gradually converged.

Fig.8 shows the cross-sectional views of the strain nephograms and distribution diagrams of the reducing section (Fig.8a), wall thickness reducing section (Fig.8b) and finishing section (Fig.8c). During cold rolling deformation, at the ridge of the pass, the stress state is composed of axial tensile strain ε_l, circumferential compressive strain ε_θ , radial tensile strain ε_r into axial tensile strain ε_l, circumferential compressive strain ε_θ and radial compressive strain ε_r. At the opening of the pass, the stress state is composed of axial tensile strain ε_l, circumferential tensile strain ε_θ, radial tensile strain into axial tensile strain ε_r, circumferential compressive strain ε_θ and radial compressive strain ε_r. Comprehensive analysis of the strain distribution cloud maps shows that the strain of the reducing section is the smallest compared to the strains of all sections, nearly zero. The strain in the wall thickness reducing section increases significantly and is unevenly distributed. The largest strain is observed in the finishing section, and the strain in the pass section is evenly distributed and the roundness is better. The overall strain variation is in accordance with the accumulation characterristics and distribution curve of equivalent plastic strain.

2.3 Temperature distribution under different rotation angles

Fig.9 reveals the node temperature distribution curves of the reducing section, wall thickness reducing section and finishing section at different rotation angles. Because no large plastic deformation occurs at the beginning of diameter reduction in the reducing section, the heat transformation is low. Moreover, the temperature difference of each node, which is close to the initial rolling temperature of 20 °C, is not significant. The node temperature increases gradually as the rolling process proceeds. Comparison of the node temperatures in different deformation stages demonstrates that the overall node temperature of the finishing section is higher than that of the reducing and wall thickness reducing sections under the same rotation angle during forming. In different deformation stages, regardless of the pass area, the node temperature increases as

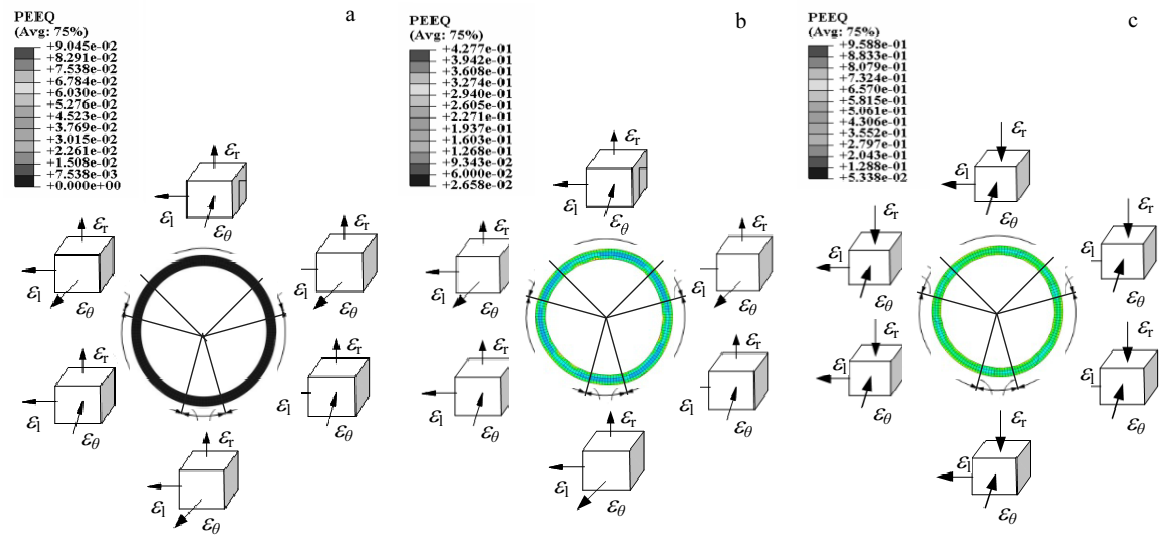

Fig.8 Schematic of the strain distributions in different deformation sections: (a) reducing section, (b) wall thickness reducing section, and (c) finishing section

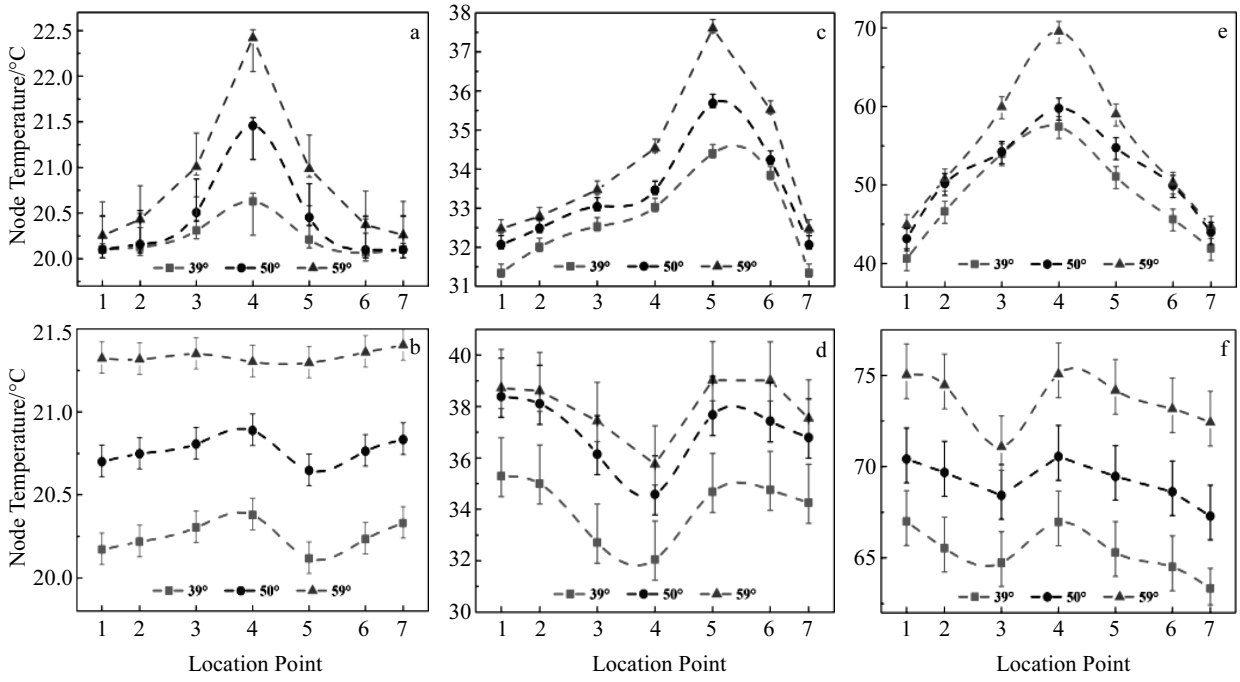

Fig.9 Temperature distribution curves of the outer wall (a, c, e) and inner wall (b, d, f) of each deformation section node at different rotation angles: (a, b) diameter reducing section, (c, d) wall thickness reducing section, and (e, f) finishing section

the rotation angle increases. Furthermore, the overall variation trend of the ridge and surroundings of the pass is larger than that of the open area of the pass.

In conclusion, when the rotation angle increases, the equivalent stress, equivalent plastic strain and node temperature of the pipe in the reducing, wall thickness reducing and finishing sections consistently increase. The maximum stress in the entire rolling process with three rotation angles does not exceed the strength limit of the AZ31 magnesium alloy tubes. The equivalent stress at a rotation angle of 59° is more favorable to rolling forming, the equivalent plastic strain in the finishing section is relatively uniform and the roundness is better. However, at a rotation angle of 59°, the temperature in the deformation area is relatively high, and the regional temperature difference is relatively large. Therefore, the resulting finished tube may have a high forming temperature

in the deformation area, leading to a decrease in its ultimate strength, cracks and other defects affecting its circumferential uniformity. According to the findings above, a 50° return angle can meet the technical requirements to ensure pipe quality.

3 Experimental Verification

3.1 Comparison of experimental results

In the current experiment, the LD40 rolling mill from a certain enterprise in Jiangsu was used for rolling. Fig.10 shows the measured and simulated results of the outer diameter of the finished tube after rolling (A-raw materials, B-reducing section, C-wall thickness reducing section, D-finishing section, E-finished section). The measured results show that the deformation state of the simulated forming process is consistent with the actual situation. In addition, the error between the average diameter measured in the experiment and the simulated average diameter is no more than 0.5 mm, which is within a reasonable range and verifies the forming accuracy of the numerical simulation model.

An infrared temperature sensor is used to conduct non-contact, real-time measurement of the temperature of the outer wall of the rolling section as a function of the rotation angles (30°, 50° and 59°) of the reducing, wall thickness reducing and finishing sections. The measurement results are shown in Fig.11.

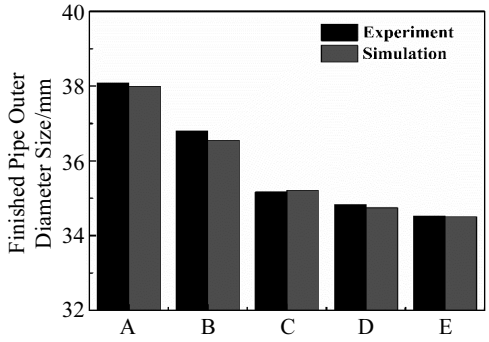

Fig.10 Comparison of experiment and simulated outer diameter

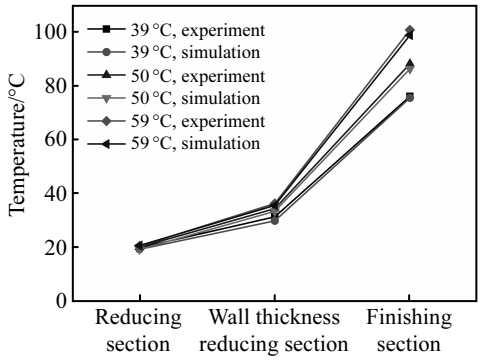

Fig.11 Comparison of the actual and simulated temperatures of the outer wall

The measured outer wall temperatures are basically consistent with the simulated values, and both increase with increasing the rotation angle, which verifies the forming accuracy of the numerical simulation model to a certain extent.

3.2 Experiment verification of microstructure

Fig.12 shows the experimental and simulated results of the average grain sizes of reducing section, wall thickness reducing section and finishing section. The average grain sizes of reducing, wall thickness reducing and finishing sections are 42.5, 32.5, 31.6 μm (experiment) and 42.88, 33.08, 31.98 μm (simulation), respectively, thereby indicating that the grain sizes are refined to a large extent during the rolling process. Furthermore, the experimental and simulated results are generally consistent.

Fig.13 shows the experimental and simulated microstructural results of reducing section, wall thickness reducing section and finishing section after rolling. The experimental results show that the overall grain distribution in the reducing section is relatively uniform. In addition, the grains have a

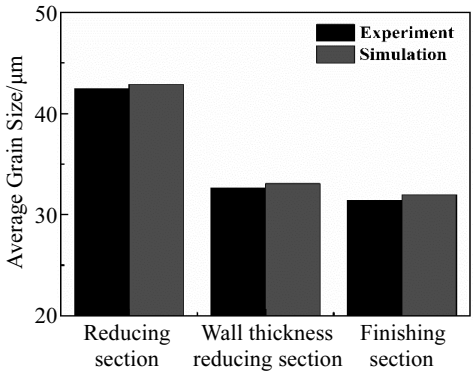

Fig.12 Experimental and simulation results of grain size

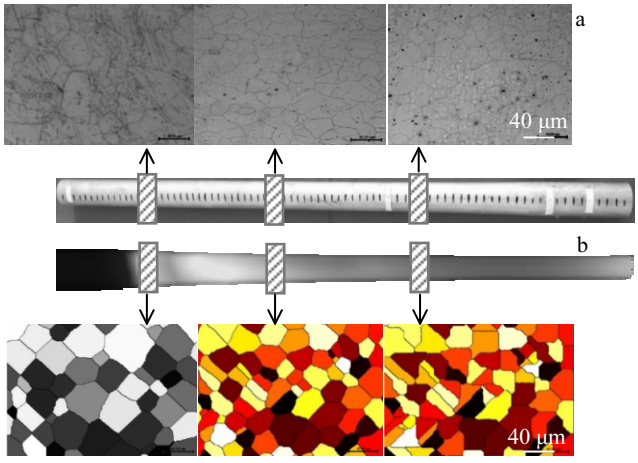

Fig.13 Experimental (a) and simulated (b) results of microstructures obtained in different deformation sections

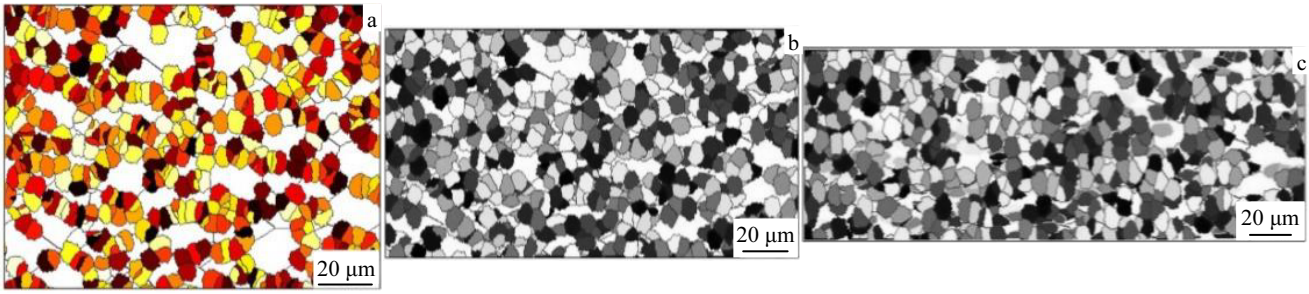

Fig.14 Dynamic recrystallization simulation results: (a) reducing section, (b) wall thickness reducing section, and (c) finishing section

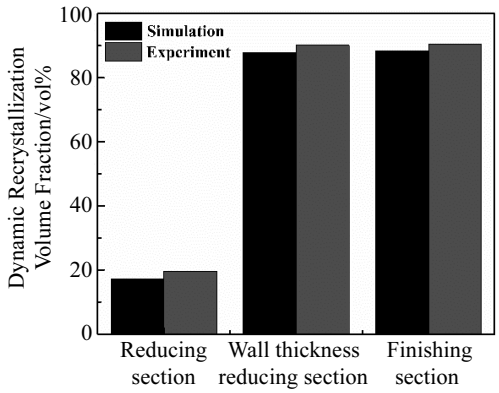

Fig.15 Dynamic recrystallized grain volume fraction of different sections of material

fairly large size and numerous twins are noted. The overall grain distribution in the wall thickness reducing section is relatively uneven, and the size and number of twins decrease. The finishing section of the whole grain reveals further homogenization, small degrees of size reduction and few twins. The simulated results show uniform grains and the absence of twins. Furthermore, because the initial state is idealized, which ignores the energy fluctuation and stacks entanglement of some parts of the material, the dislocation and energy distributions are uniform. Overall, the experimental results are consistent with the simulation results.

Fig.14 shows the simulation results of the dynamic recrystallization of samples reducing section, wall thickness reducing section and finishing section. Here, primary grains are gradually replaced by fine recrystallized grains as deformation proceeds.

Fig.15 shows the measured dynamic recrystallized grain volume fractions of samples. Results show that the volume fraction of recrystallized grains in reducing, wall thickness reducing and finishing sections is 19.5 vol%, 90.1 vol%, 90.5 vol% (experiment) and 17.24 vol%, 87.90 vol%, 88.331 vol% (simulation), respectively. This phenomenon may be explained as the rolling process progresses, the temperature, and the thermal activation of recrystallization need can increase, grain boundary migration rate is accelerated, and recrystallization grain volume fraction increases. The experimental and simulation results are basically identical.

4 Conclusions

1) The improvement of mechanical properties and temperature in the process of metal forming is obtained through studies of different rotation angles during three-roll cold-rolling. The equivalent stress, equivalent plastic strain and node temperature of the pipe increase with increasing the rotation angle, and the optimal process parameter, namely, a return angle of 50°, is obtained by comprehensive analysis of various factors

2) The cellular automaton model can be used to predict the formation of continuous recrystallization grains during the rolling process and refinement of the initial structure evolution law, through the experiment and simulation results contrast, from outside diameter size, the outer wall temperature and grain size. The rationality of the selected rotation angle is verified.

References

1 Zhang H Q, Wang X F, Wei B L *et al*. *The Int J Adv Manuf Technol*[J], 2017, 92(5-8): 2169
2 Pociecha D, Boryczko B, Osika J *et al*. *Arch Civ Mech Eng*[J], 2014, 14(3): 376
3 Li Heng, Wei Dong, Yang Heng *et al*. *Aeronautical Manufacturing Technology*[J], 2018, 61(21): 16 (in Chinese)
4 Gurao N P, Akhiani H, Szpunar J A. *Journal of Nuclear Materials*[J], 2014, 453(1-3): 158
5 Stinnertz H. *Tube Pipe Technology*[J], 1988, 2(7): 27
6 Lodej B, Niang K, Montmitonnet P *et al*. *Journal of Materials Processing Technology*[J], 2006, 177(1-3): 188
7 Osika J, Libura W. *Journal of Materials Processing Technology* [J], 1992, 34(1-4): 325
8 Danchenko V N, Frolov Y V, Dekht-Yarev V S *et al*. *Metallurgical and Mining Industry*[J], 2011, 3(3): 110
9 Montmitionnet P, Logé R, Hamery M *et al*. *Journal of Materials Processing Technology*[J], 2002, 125-126: 814

10 Abe H, Iwamoto T, Yamamoto Y *et al*. *Journal of Materials Processing Technology*[J], 2016, 231: 277
11 Huang Liang, Xu Zhe, Dai Chun *et al*. *Rare Metal Materials and Engineering*[J], 2013, 42(3): 524 (in Chinese)
12 Huang Liang, Xu Zhe, Dai Chun *et al*. *Rare Metal Materials and Engineering*[J], 2013, 42(4): 741 (in Chinese)
13 Chu Zhibing, Lu Yangyang, Huang Qingxue *et al*. *Advanced Engineering Sciences*[J], 2015, 47(2): 165 (in Chinese)
14 Guo Changhai. *Thesis for Master*[D]. Hohhot: Inner Mongolia University of Science and Technology, 2014 (in Chinese)
15 Ji Haipeng. *Dissertation for Doctorate*[D]. Qinhuangdao: Yanshan University, 2013 (in Chinese)
16 He Dong. *Thesis for Master*[D]. Harbin: Harbin Institute of Technology, 2007 (in Chinese)
17 Chu Zhibing, Zhang Duo, Jiang Lianyun *et al*. *Rare Metal Materials and Engineering*[J], 2018, 47(3): 884 (in Chinese)
18 Zheng Yi. *Thesis for Master*[D]. Taiyuan: Taiyuan University of Science and Technology, 2015 (in Chinese)
19 Xiao Namin, Zheng Chengwu, Li Dianzhong *et al*. *Computational Materials Science*[J], 2008, 41(3): 366
20 Ding R, Guo Z X. *Acta Materialia*[J], 2001, 49(16): 3163

回转角对 AZ31 镁合金管材冷轧成形过程的影响

薛　春[1]，楚志兵[1,2]，苏　辉[1]，李　伟[1]，李玉贵[1]，马立峰[1]
(1. 太原科技大学 重型机械教育部工程研究中心，山西 太原 030024)
(2. 暨南大学 力学与建筑工程学院，广东 广州 510632)

摘　要：以冷轧 AZ31 镁合金管材为研究对象，对不同回转角下的冷轧过程进行了完整的仿真，对比分析了不同回转角在各特征变形阶段对等效应力、等效塑性应变及节点温度的影响规律。结果表明，随着回转角的增大，等效应力、等效塑性应变以及节点温度均增大。借助元胞自动机模型以及实验等手段，通过实验与数值仿真结果对比分析，探明了晶粒在轧制过程中产生连续再结晶并细化的初步组织演变规律，并发现 50°的回转角可以更好的满足工艺要求。本研究可为镁合金管材冷轧成形回转角的选择提供依据。

关键词：三辊式冷轧；回转角；数值仿真；元胞自动机

作者简介：薛　春，男，1994 年生，硕士生，太原科技大学重型机械教育部工程研究中心，山西 太原 030024，E-mail: 844924572@qq.com